




## Research Article

# Full-Scale Model Experimental Study of the Flexural Behavior of Hollow Slabs Strengthened by UHPC

Jinzi Zhou <sup>1,2</sup>, Zihao Wen,<sup>1</sup> Weiqi Mao,<sup>2,3</sup> Chuheng Zhong <sup>1</sup>, Kangning Wang,<sup>2,3</sup>  
and Chenxu Zhou <sup>1</sup>

<sup>1</sup>School of Civil Engineering Architecture and Environment, Hubei University of Technology, 430068 Wuhan, China

<sup>2</sup>China State Key Laboratory for Health and Safety of Bridge Structures, 430034 Wuhan, China

<sup>3</sup>China Railway Major Bridge Engineering Group Co., Ltd., 430050 Wuhan, China

Correspondence should be addressed to Chuheng Zhong; [chuheng.zhong@hbut.edu.cn](mailto:chuheng.zhong@hbut.edu.cn)

Received 26 February 2021; Accepted 20 September 2021; Published 11 October 2021

Academic Editor: Youyou Zhang

Copyright © 2021 Jinzi Zhou et al. This is an open access article distributed under the Creative Commons Attribution License, which permits unrestricted use, distribution, and reproduction in any medium, provided the original work is properly cited.

The hollow slabs strengthened by ultrahigh performance concrete (UHPC) composite beam show many advantages over traditional reinforcement methods. In this paper, full-scale model load tests were carried out on a nonstrengthened prestressed concrete hollow slab and an UHPC-strengthened prestressed concrete hollow slab, comparing the load deflection, crack width, bearing capacity, deformation resistance, and self-vibration frequency of the two. Static loading experimental results indicate that UHPC enhances the overall performance of prestressed concrete hollow slabs by decreasing deflection and crack width and improving bearing capacity. The strengthening effects of UHPC on a prestressed concrete hollow slab's flexural behavior are also discussed, such as deflection, crack width, bearing capacity, deformation resistance, self-vibration frequency, flexural behavior, and cracking load. Deflection and crack width under a load of 800 kN decreased by 45.8% and 56.3%, respectively, and the initial self-vibration frequency, ultimate bearing capacity, and cracking load increased 19.2%, 21.4%, and 50%, respectively. The plane assumption can be made generally throughout the overall test process while using UHPC strengthening, which significantly constrains crack width and improves stiffness and deformation capacity. The UHPC layer and the prestressed concrete hollow slab were connected by shear studs to produce a good composite action between them, and the bending performance and bearing capacity of the whole structure were clearly improved. In addition to experiments, a validated numerical model is developed to verify the flexural performance of hollow slab strengthened by UHPC.

## 1. Introduction

Prefabricated reinforced concrete or prestressed concrete hollow slab is widely used in the construction of expressways and urban bridges, because it offers the advantages of standardized design, integrated production, assembly construction, low cost, low building height, overall beauty, clear structure force, and so on. Owing to their lower design load standards, the flexural behavior of bridges built in the 20th century reserve reduces driving safety and affects the normal operation of highway and urban road traffic. Maintenance and rehabilitation of highway bridge decks is a continual challenge for bridge owners and transportation agencies. Transportation agencies must extend the service lives of existing bridge decks using limited funds, with limited time

needed for replacement or major rehabilitation. The deterioration associated with bridge diseases is progressive and irreversible. Resilient and durable repair and rehabilitation solutions are urgently needed for these aging reinforced concrete bridge decks.

Common reinforcement methods include active strengthening and passive strengthening. Passive strengthening includes pasting steel plate [1], carbon fiber board, and the like, but passive strengthening material can bear only the internal forces caused by an active load. Active strengthening, by contrast, requires that the sticking strengthening material be prestressed to form a prestressed reinforcement system, which can improve the utilization rate of strengthening materials—a method widely used in bridge strengthening. The most common prestressed reinforcement

materials include prestressed steel strand, steel wire, steel wire rope, and fiber-reinforced polymer (FRP). FRP, which has the advantages of heat resistance and corrosion resistance, has been widely used to reinforce concrete bridges, but after strengthening, the beam's ductility decreases, and the beam often exhibits brittle failure [2–6]. Prestressed steel strand and steel wire have good ductility, are cost-efficient, and bond well with concrete, advantages that make them suitable for use in prestressed concrete bridges [7–10]. Hui Peng et al. [11] pointed out that externally bonded prestressed FRP plates and near surface-mounted (NSM) FRP strips represent two important techniques for strengthening concrete structures with FRP materials. However, they have considerable limitations. Prestressed NSM FRP strips combine the advantages of these two strengthening methods and are thus an extremely attractive approach to using FRP to retrofitting concrete structures. Although prestressed FRP strips can be anchored by epoxy through near-surface mounting, the failure modes of beams strengthened through this technique could include debonding of the epoxy-concrete interface and delamination of the concrete cover. These failure modes can be avoided by extending the bond length of FRP strips or using U-wraps of carbon fiber reinforced polymer (CFRP) sheets. Al-osta M A et al. [12] studied the reinforcement effect of various interface treatment methods and reinforcement positions on reinforced concrete beams, finding a higher interface bonding performance for the sandblasting interface treatment method, with the U-shaped hoop reinforcement the most suitable reinforcement method for not only improving the bending capacity by 89%, but also reducing members' midspan deflection by 20% compared with that of unreinforced members'.

Ultrahigh performance concrete (UHPC) is a new type of cement-based composite material that has ultrahigh durability and mechanical properties. UHPC material should be used in places chosen to reflect its ultrahigh strength, ductility, and durability, consistent with the basic principles of UHPC reinforcement [13]. Bridge structure systems differ, whether in structure environment, main load form, or reinforcement demands. Beam and slab structures are subjected mainly to bending and shear forces, and their bearing capacity is often accompanied by midspan deflection along with other diseases. Their reinforcement thus focuses on improving their bending bearing capacity and restraining their further deflection [14]. Muhammad Safdar et al. [15, 16] used UHPFRC material to replace the top and bottom parts of reinforced concrete beams, effectively enhancing NC beams' bending capacity. Because ultimate bearing capacity is still determined by longitudinal reinforcement at the bottom of a beam, H. M. Tanarlsan [17] used a thin precast UHPC layer to strengthen reinforced concrete beams. Although affixing UHPC thin layer at the bottom of a beam can effectively enhance the ultimate bearing capacity of strengthened members, their deflection is also difficult to control. Hor Yin et al. [18] used UHPC material to strengthen a reinforced concrete slab and found that a reinforced concrete slab strengthened by UHPC at its bottom could effectively inhibit development of cracks in strengthened components during bending shear, effectively

improving the structure's bending bearing capacity. Zmetra et al. [19] proposed a novel repair method for steel girder ends with corrosion damage, using UHPC to encase the corrosion. For this repair, UHPC panels were attached to girders with shear studs welded to the web and flange surrounding the corroded area, allowing shear and bearing forces to transfer from the girder to the UHPC panels. The UHPC panels provided a new load path, increasing the bearing capacity of the girder. Gaston Doiron et al. [20] suggested that the UHPC's durability can contribute to other types of bridge repairs and provided a brief overview of four North American pier repair/retrofit projects.

Xu et al. [21] used UHPC mixed with polymer fiber to strengthen plain concrete beams by using a cast-in-place plain UHPC layer to reinforce their underside, greatly improving their bending capacity while inhibiting the development of cracks. Wu and Lin [22] evaluated the influence of U-shaped UHPC reinforcement over the failure mode, fracture strength, ultimate bearing capacity, and deformation of RC beams. Qi [23] carried out UHPC reinforcement tests on three full-scale box girder roof local models and found that, under positive and negative bending moments, reinforcement could effectively improve the overall stiffness of the specimen, which exhibited good ductility and obvious deformation before failure. Liu et al. [24], who proposed pouring a layer of UHPC atop the bridge deck, carried out theoretical and experimental research and found that the lateral strain and vertical deflection of the bridge deck were reduced by about 60%, with the stress also being reduced under the action of vehicle load, and that the UHPC layer could effectively improve the stress of the bridge deck. Deng and Zhang [25] verified that the bottom of a reinforced concrete beam strengthened with a thin layer of UHPC exhibited greatly improved bending capacity and reduced midspan deflection. Yang and Zhi [26] studied the flexural behavior of UHPC beams and found that UHPC showed good compression performance, good ductility, and ultimate deformation capacity. Zhang et al. [27] conducted an experimental study of the flexural capacity of RC beams and found that newly fabricated integral RC beams had the same flexural capacity as cast-in-place RC beams, with good integrity and ductility. Zhu et al. [28] analyzed the different failure modes of UHPC-RC composite members under bending deformation, conducting static load tests of RC beams strengthened with UHPC, and found that UHPC can be used to improve the flexural strength of RC beams or slabs. In addition, cost analysis against other strengthening technologies (such as CFRP) is proposed by them. Finally, they suggested some examples to guide applications of reinforced concrete structure UHPC strengthening technology.

UHPC-strengthened hollow slabs have been used in engineering, but the research on the bending properties of hollow slabs, such as the strengthening effect of UHPC and improvements to bending capacity, has involved only solid beams and scale model beams, which cannot effectively guide the design and application of UHPC-strengthened hollow slabs. Accordingly, full-scale model tests of bending performance of UHPC-reinforced hollow slab bridges would

be theoretically significant while having practical value for engineering.

The purpose of this paper is to study the influence of UHPC strengthening on the bearing capacity, crack inhibition, bending stiffness, flexural behavior, natural frequency, and overall consistency of prestressed concrete hollow slabs through full-scale model testing while theoretically calculating cracking load and bearing capacity, to prove that UHPC has a notable strengthening effect on prestressed concrete hollow slabs. In addition, a numerical analysis is carried out to further analyze the flexural performance of hollow slab strengthened by UHPC.

## 2. Full-Scale Model Test

**2.1. Axial Tensile Test.** For axial tensile test, the embedded axial tensile specimen, UHPC with the size of  $100\text{mm} \times 100\text{mm} \times 500\text{mm}$ , is selected. 12.9-grade  $\text{Ø}16$  screw is used for embedded rod. By setting the screw to full length, the UHPC is indirectly stretched by the screw. When tensile microcracks appear in UHPC, the axial force gradually transfers to the screw, which can effectively avoid the sudden release of elastic potential energy. The axial force of UHPC can be obtained indirectly by measuring the tensile force of the testing machine and the axial force of the screw (measured by the strain gauge attached to the screw), so as to determine the relationship between the nominal stress and the nominal strain in the whole process. Before the test, three screws of the same batch are stretched (for calibration). The tensile strain should be controlled at  $4000 \mu\epsilon$ , and the screw load  $F_L$ -strain  $\epsilon_L$  corresponding relation is measured; the actual length and width values of the two sections of the axial tensile section of the specimen are measured to calculate the average value  $a$  of the section area; the strain gauge is pasted longitudinally at the center of four sides of the specimen, the strain tester is connected, and the steel bracket and dial indicator are arranged at the two opposite tension sections of the face axis; the pretension force is set to 10 kN, 15 kN, and 20 kN. After the pretension force is loaded to the value, the alignment of the specimen is checked. During the formal loading, the whole process is controlled by displacement. Before 60 kN, the speed is 0.005mm/s. After 60 kN, the tensile speed is 0.002mm/s until the screw is broken. Based on the measured screw strain  $\epsilon_L$ , the screw axial force  $F_L$  can be converted, and then the UHPC axial force  $F_U$  can be calculated from the difference between the tensile force  $F$  of the testing machine and the screw axial force  $F_L$ , from which the nominal stress  $\sigma$  and nominal strain  $\epsilon$  relationship can be calculated in the whole process of UHPC tension.

**2.2. Sample of Hollow Slab.** Three prestressed concrete hollow slabs used in the test were prefabricated in a factory. The material list is shown in Table 1.

The detailed dimensions of the tested prestressed concrete hollow slab are shown in Figure 1. The three hollow slabs are denoted as S1, S2, and S3: Specimen S1 is not strengthened, Specimen S2 has UHPC strengthening at the top, and Specimen S3 has UHPC strengthening at the top

and CFRP strengthening at the bottom. The prestressed concrete hollow slab and the UHPC panel were connected by the shear studs 19 mm in diameter and 150 mm long. The geometric dimensions, reinforcement, and shear stud arrangements of Specimens S2 and S3 are shown in Figure 2. Due to the placement of steel bars and arrangement of vertical and horizontal steel mesh in the inner layer, the thickness of one layer of steel mesh is 10 mm, plus a 15 mm thick protective layer, and the thickness of UHPC is 50 mm, with two layers of steel mesh and two protective layers. The shear stud length, UHPC hierarchical structure, and sticking position of CFRP are shown in Figure 3.

**2.3. Four-Point Bending Test.** The four-point bending tests of Specimens S1, S2, and S3 were carried out on the testing machine, with an MTS hydraulic loading system being used for load. The positions of strain gauge measuring points on the specimen and the arrangement of electronic displacement meters are shown in Figure 4. The strain gauges were glued on the concrete. During the test, the deflection and strain were monitored in midspan, at the loading point, and near the support. The length of pure bending deformation is 3 m in the middle section of the specimen, and the shear span ratio is 5.3. The four-point bending tests are shown in Figure 5.

Before loading, the specimen must be preloaded to confirm that the measuring device and loading device are working normally. In the test, graded loading is adopted, with the force controlled first and the loading carried out at 0.2 kN/s. Before the loading reaches the estimated cracking load of the specimen, it is changed to graded loading, with an increment not more than 10 kN. When the specimen cracks, the increment of graded loading is changed to 5% of the predicted ultimate load. When approaching the ultimate load, the force control loading is changed to displacement control loading, with loading proceeding gradually until the specimen is damaged.

## 3. Test Results and Discussion

**3.1. Axis Tensile Strength.** As shown in Table 2, the tensile test results of UHPC are shown in the figure, and the tensile strength is 7.4 MPa. As shown in Figure 6, uniaxial tensile of UHPC material has strain hardening characteristics, and the stress-strain curve of the whole uniaxial tensile process can be simplified into three stages: (1) linear elastic stage: the initial crack strain  $\epsilon_{cr}$  is regarded as the termination mark there, and it is obtained from the ratio of tensile strength  $f_{tk}$  to elastic modulus  $E_c$ ; (2) the formation stage of matrix material cracking and dispersive microcracks in UHPC, marked by yield ultimate tensile strain  $\epsilon_{tu}$ ; (3) formation and development of macro main fracture and the decline stage of steel fiber being pulled out, marked by ultimate tensile strain  $\epsilon_u$ .

**3.2. Load-Deflection Response.** Four-point bending tests of S1, S2, and S3 were carried out. A comparison of the maximum deflection of Specimens S1, S2, and S3 in the

TABLE 1: Material list.

Material	Concrete	Prestressed reinforcement	Prestressed steel strands	UHPC	CFRP
Model	C45	HRB335 $\Phi$ 12 mm	4 $\Phi$ s15.2	UHPC120	CFRP (0.167 mm)

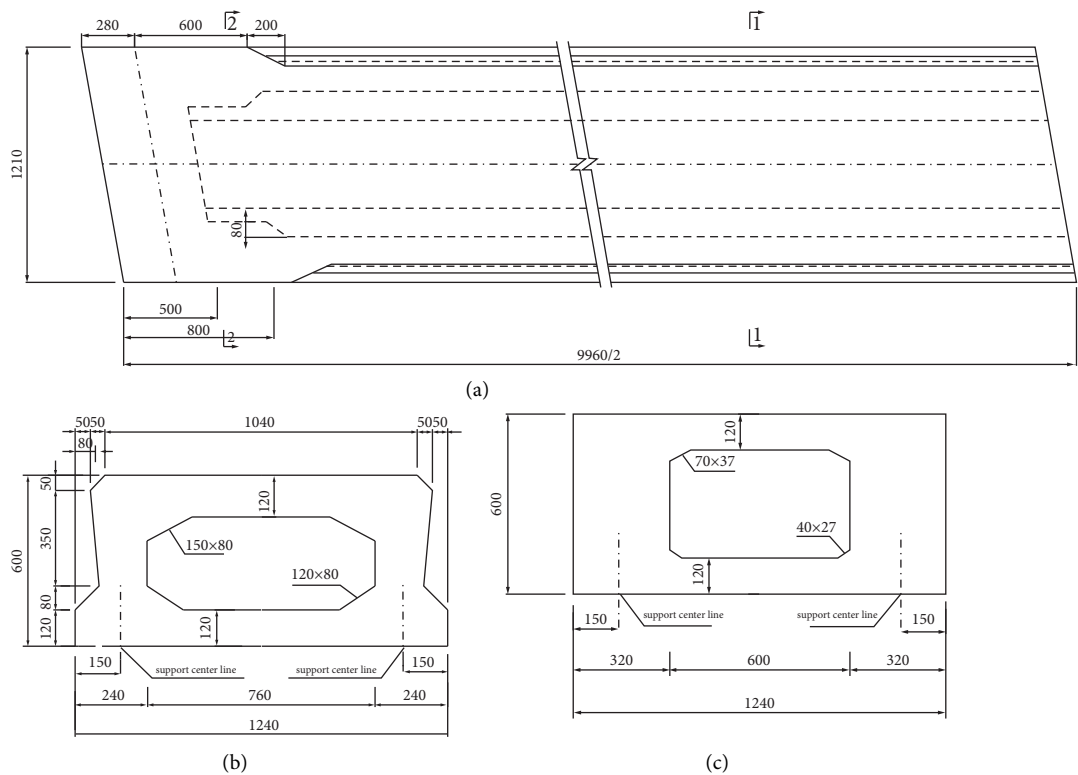


FIGURE 1: Structural drawing of the hollow slab beam. (a) Plan view. (b) Section 1-1. (c) Section 2-2.

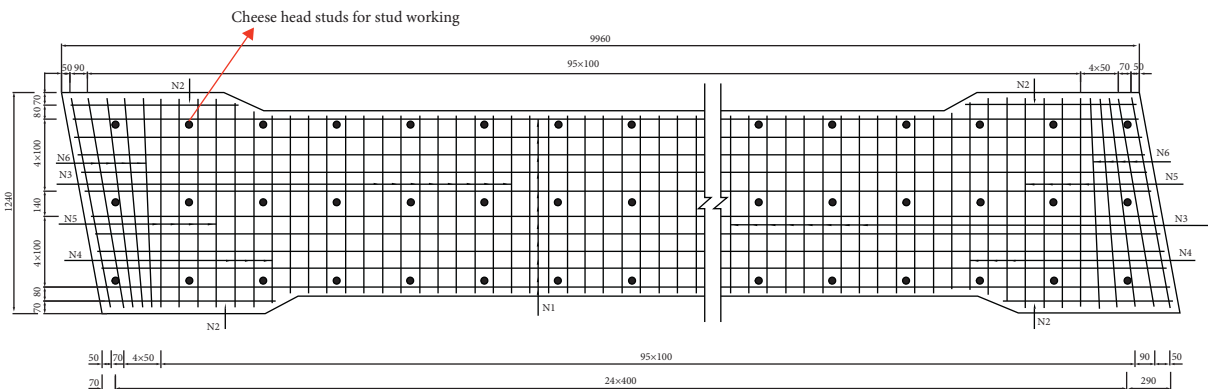


FIGURE 2: Layout of welding pin position on UHPC panel.

middle span during testing is shown in Figure 7. The load-deflection relationship in the midspan span of three samples S1, S2, and S3 during the test is shown in Figure 8. The failure phenomena of S1, S2, and S3 at the end of the test are shown in Figure 9.

Figures 7 and 8(a) show obviously smaller midspan deflections of Specimens S2 and S3 than of Specimen S1 at the same load level, a phenomenon more obvious with increased load, which indicates that the midspan deflection

of prestressed concrete hollow slabs can be controlled by UHPC strengthening. Under 800 kN load, the midspan deflection of UHPC-strengthened prestressed concrete hollow slab is about 45.8% lower than that of without strengthened prestressed concrete hollow slab. The stiffness of UHPC-strengthened prestressed concrete hollow slab is greater than that without strengthened prestressed concrete hollow slab, indicating that UHPC strengthening can effectively improve the stiffness of prestressed concrete hollow

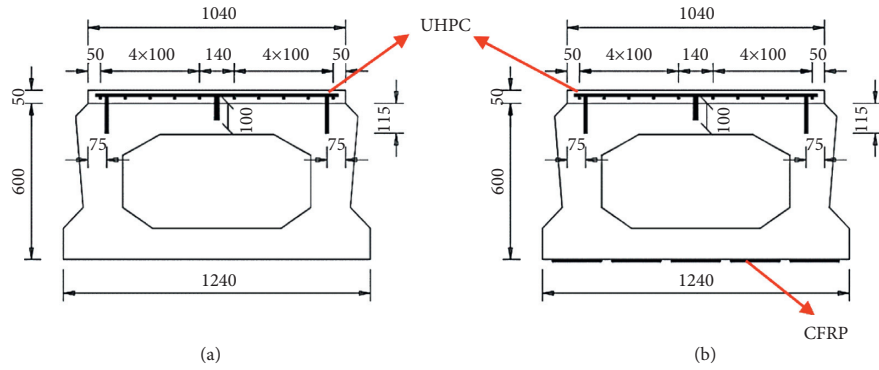


FIGURE 3: Midspan cross section of Specimen S2 and S3. (a) Specimen S2. (b) Specimen S3.

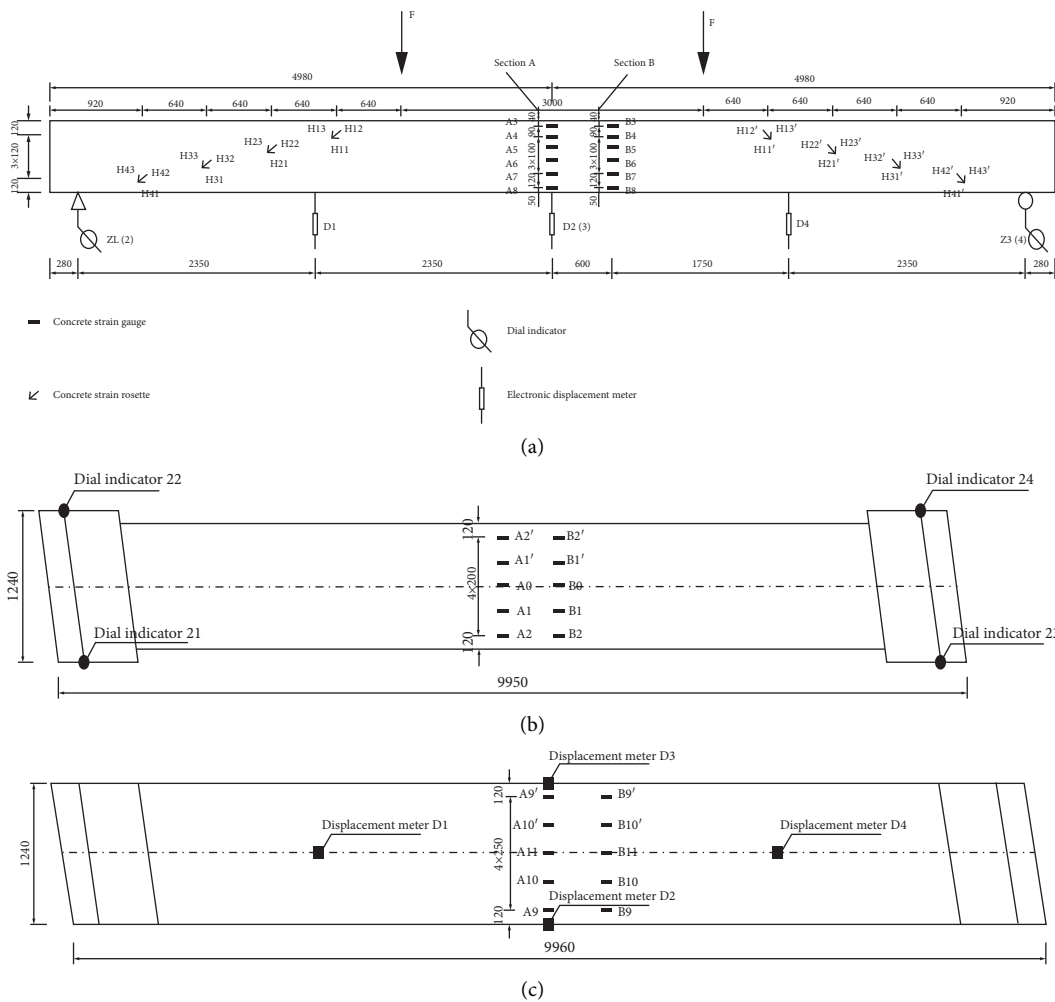


FIGURE 4: Layout of measuring points on the sample. (a) Elevation of the specimen. (b) Top view of the specimen. (c) Bottom view of the specimen.

slab. The maximum deflection of Specimens S2 and S3 exceeded that of Specimen S1 by 119% and 81.9%, respectively, with the ductility of Specimen S2 exceeding that of Specimen S3, indicating that the strengthening effect of CFRP mainly improves the tensile capacity of steel bars. From Figure 7(a), it can be seen that the ultimate bearing capacities of Specimens S1, S2, and S3 were 838 kN,

1,017 kN, and 1,060 kN, respectively. Compared with S1, the increments of S2 and S3 were 21.4% and 26.5%, respectively.

From the load-deflection curve of the prestressed concrete hollow slab (Figure 8(a)), it can be seen that, from the beginning of loading to failure, the prestressed concrete hollow slab successively experiences three different stress processes: the linear elastic stage, crack stage, and failure stage.

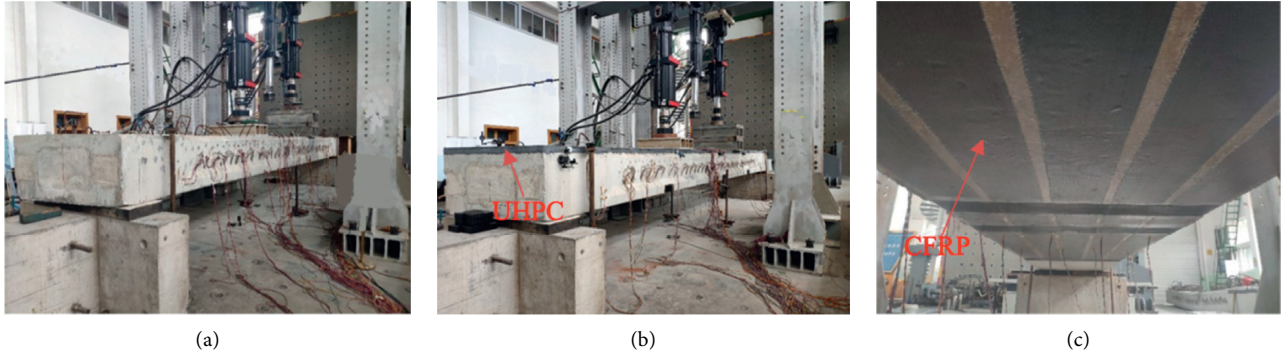


FIGURE 5: Four-point bending tests. (a) Specimen S1. (b) Specimen S2. (c) Specimen S3.

TABLE 2: Tensile testing results.

Specimens	$F_U$ (kN)	Sectional area (mm <sup>2</sup> )	Tensile strength (MPa)
BGGX-1	73.0	9,851.0	7.4
BGGX-2	77.5	9,906.3	7.8
BGGX-3	69.3	9,866.0	7.0

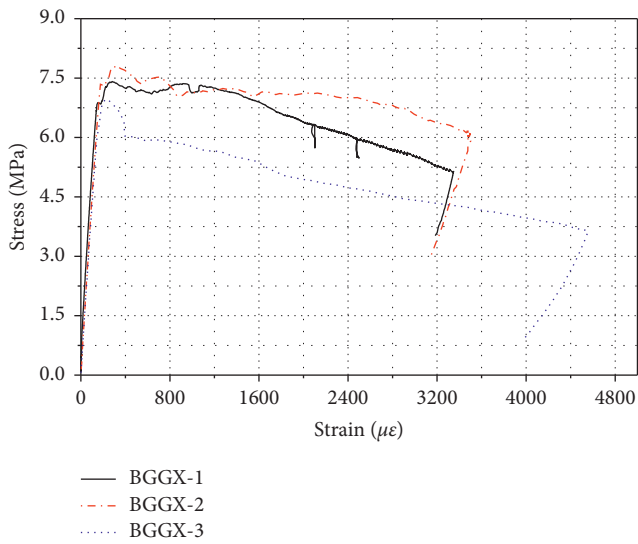


FIGURE 6: UHPC stress-strain curve.

In the linear elastic stage, from the beginning of loading to the initial cracking of the prestressed concrete hollow slab, the ratio of loading to deformation increases linearly. At the beginning, there is no cracking in the prestressed concrete hollow slab. As load increases, discontinuous cracks appear in its interior. According to data measured by the strain gauge affixed to the surface of the prestressed concrete hollow slab, the neutral axis moves up continuously. At this stage, the deformation of the prestressed concrete hollow slab is caused mainly by the elastic deformation of aggregate and cement crystal in concrete, whereas the viscous flow of cement colloid and the change of initial crack have little influence, and the load-deflection curve is approximately linear. When the tensile strain of the tensile edge reaches the ultimate tensile strain of concrete ( $\epsilon_t = \epsilon_{ut}$ ), the prestressed

concrete hollow slab is in the critical state of cracking ( $I_a$  state); the load at this time is called “cracking load.”

Then, the specimen enters the cracking stage. In this stage, with the increase of load, the concrete in the tensile stress zone essentially does not take effect, with the tensile stress borne mainly by the longitudinal tensile steel bar, which does not yield. The relationship load-midspan deflection is a curve, gently sloped until the tangent of the curve is horizontal, and the tensile steel bar yields.

When the tensile reinforcement yields, the tensile stress remains constant, and the bearing capacity of the UHPC-strengthened prestressed concrete hollow slab increases very slowly. During this period, the action point of the combined pressure on the concrete in the compression zone moves outward, and the internal force arm and bending moment increase. The compressive strain of the concrete at the edge of the compression zone reaches the ultimate compressive strain, the concrete is crushed, and the members enter the failure stage. The load-deflection curve is close to being horizontal.

Figure 8(b) shows that the cracking loads of Specimens S1, S2, and S3 are 200 kN, 300 kN, and 300 kN, respectively. The increasing amplitudes of Specimens S2 and S3 are identical, at 50%. UHPC strengthening can improve not only the bearing capacity of a prestressed concrete hollow slab, but also its plasticity, so that UHPC can be used to strengthen a prestressed concrete hollow slab.

According to the analysis in Figure 9, after the failures of Specimens S2 and S3, no extrusion was evident on the surface of UHPC panel, whereas the top concrete surface of Specimen S1 was damaged. Specimens S1, S2, and S3 all showed the failure of bending capacity: the tensile steel bars entered the yield state, and the concrete in the compression zone was crushed.

**3.3. Section Strain before Cracking.** During the test, the strain at the middle sections of Specimens S1, S2, and S3 along the section height was measured before the concrete tensile cracking occurred, as shown in Figure 10. From Figure 10, the distribution of strain along the section height of the three groups of specimens satisfies the plane section assumption, with the measured value of neutral axis height being essentially consistent with the theoretical value (see

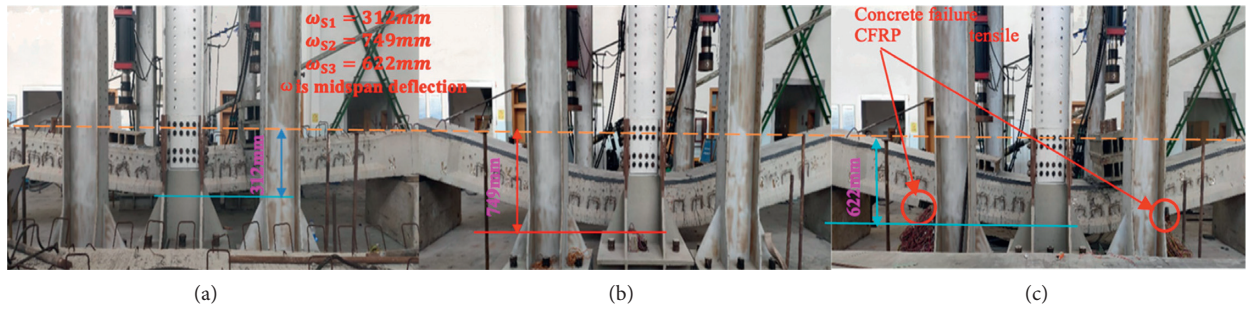
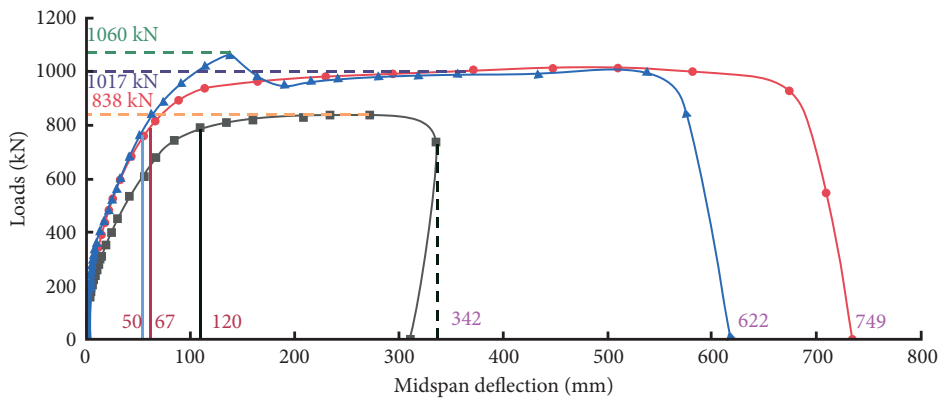
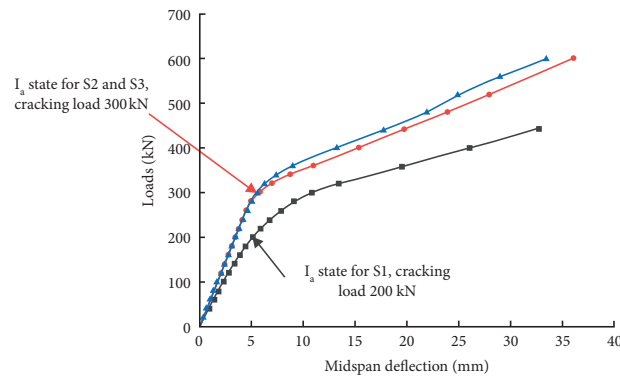


FIGURE 7: Comparison of maximum deflection of Specimens S1, S2, and S3 in the middle span during testing. (a) Specimen S1. (b) Specimen S2. (c) Specimen S3.



- S1
- S2 (UHPC)
- ▲ S3 (UHPC+CFRP)

(a)



- S1
- S2 (UHPC)
- ▲ S3 (UHPC+CFRP)

(b)

FIGURE 8: Load-deflection curve in midspan. (a) The whole process of the test. (b) Stage I: uncracked stage.

Table 3 neutral axis height), but the neutral axis of sample S1 is lower than that in samples S2 and S3. The neutral axes of samples S2 and S3 are quite close in Figure 10(b), with notably good bonding between the UHPC parts of samples S2 and S3 and the prestressed concrete hollow slab, showing good composite effect, and exceptionally good performance of the composite part.

3.4. Comparison of Crack Width. The relationship between the maximum crack and load of Specimens S1, S2, and S3 is shown in Figure 11. During testing, when studying the cracking process of Specimen S2, the strain gauge data of Specimen S2 changed when load  $F = 300$  kN, with cracks seen in the front corner of the sample bottom plate, 0.02 mm wide. When load  $F = 320$  kN, the cracks



FIGURE 9: Failure of specimens S1, S2, and S3. (a) Sample S1: roof. (b) Sample S2: breaking of reinforcement. (c) Sample S3: collapse of UHPC.

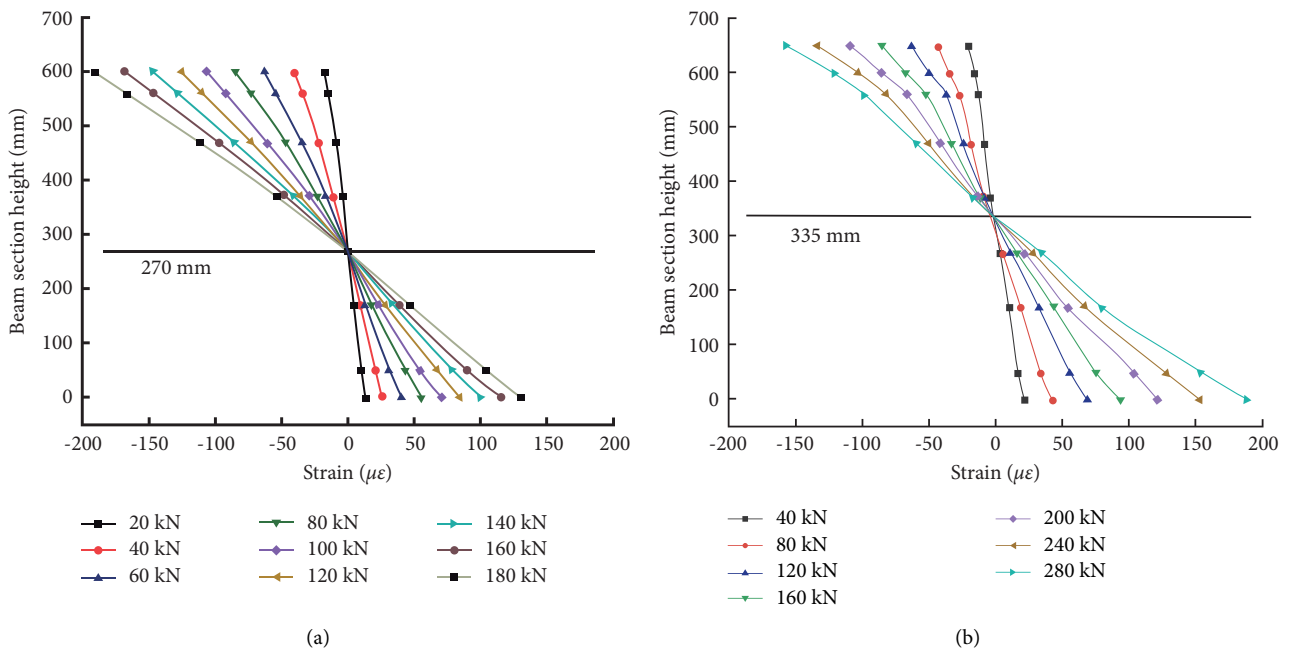


FIGURE 10: Strain distribution at the midspan section. (a) Sample S1. (b) Samples S2 and S3.

expanded rapidly, with 2~3 through cracks on the bottom surface that then expanded into a net shape, with a maximum crack on the bottom surface of 0.13 mm and a maximum crack on the side of 0.05 mm. When load  $F = 500$  kN, some cracks penetrated the roof but had not extended into UHPC, in the compression zone; obvious crack openings occurred but did not extend to the UHPC layer. When the load reached the limit load, the strain

gauge between the UHPC and the concrete was damaged, and a certain strain deviation was seen.

The cracking processes of Specimens S1 and S3 are like those of Specimen S2, but the cracking load of Specimen S1 is smaller than that of Specimen S2. Figure 11 shows that the crack inhibition of Specimens S2 and S3 is improved to a certain extent and that crack propagation is slow. CFRP has little effect on the initial cracking load but can prevent crack



TABLE 3: The calculation results of cracking load.

Specimens	Conversion area (mm <sup>2</sup> )	Convert the moment of inertia (mm <sup>4</sup> )	Height of neutral axis (mm)	Cracking moment (kN·m)	Cracking load (kN)
S1	459,912	1.91E + 10	287.5	577	180
S2	526,612	2.58E + 10	330.2	915.2	286
S3	526,612	2.58E + 10	330.2	915.2	286

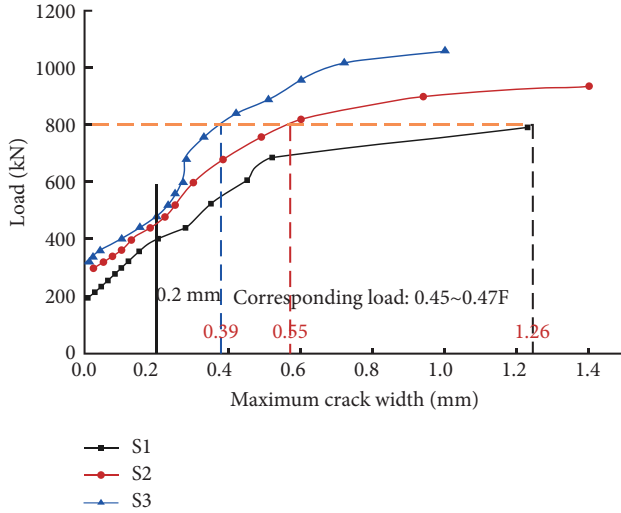


FIGURE 11: Load-maximum crack width curve.

propagation. Under 800 kN load, the crack widths of Specimens S2 and S3 decrease 56.3% and 69%, respectively. When cracking reaches 0.2 mm, the load is 0.45–0.47 of the ultimate bearing capacity.

**3.5. Effect of Crack on Natural Frequency.** UHPC strengthening has a certain influence on the natural frequency of prestressed concrete hollow slabs, as shown by the test results in Figure 12. The initial natural frequency of Specimen S3 increased 19.2%, with little change in natural frequency before the maximum crack width reached 0.2 mm. However, when the maximum crack width reached 0.2 mm, the natural frequency changed greatly.

#### 4. A Method for Calculating the Flexural Capacity of a Normal Section

**4.1. Ultimate Bearing Capacity.** Taking Specimen S1 as an example to deduce the formula for calculating bearing capacity, we assume that it conforms to the plane section assumption before reaching ultimate load, the concrete in tensile zone does not bear tensile force, the relationship curve of compressive stress and compressive strain of concrete is as shown in Figure 13(a), the stress and strain curve of tensile reinforcement is as shown in Figure 13(b), and the ultimate tensile strain is 0.01. By solving the equilibrium equation, the bearing capacity of Specimen S1 can be calculated.

Because the compression area of the section is reinforced based only on the structural requirements, the prestressed reinforcement in the compression area and the influence of

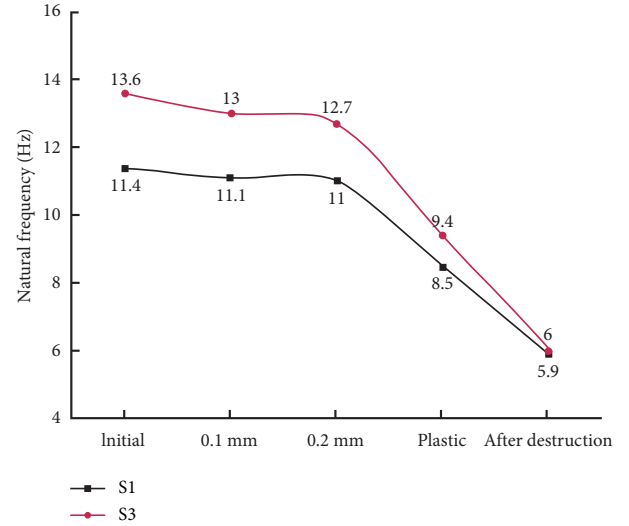


FIGURE 12: Effect of crack on natural frequency.

ordinary reinforcement are not considered in the calculation.  $A_s = 1,357.2 \text{ mm}^2$ ,  $a_s = 50 \text{ mm}$ ,  $A_p = 1,120 \text{ mm}^2$ , and  $a_{sp} = 85 \text{ mm}$ .  $A_s$  is 12 longitudinal tensile bars' area,  $a_s$  is the distance between the steel bar and the concrete edge of the prestressed concrete hollow slab,  $A_p$  is two prestressed steel strands' area, and  $a_s$  is the distance between prestressed concrete hollow slab and the concrete edge of the prestressed concrete hollow slab. When Specimen S1 is damaged, the steel bars and prestressed steel strands in the tensile stress zone reach the yield strength, and the environment is class I.

According to the principle of equal area and equal moment of inertia, Specimen S1's normal section in the midspan is converted into an equivalent I-section, as shown in Figure 14:

The distribution of bending internal force on the normal section is shown in Figure 15, where  $x$  is the height of the compression zone on the section  $x < h'_f$ .

Based on the static equilibrium equation  $\sum F_x = 0$ , it can be shown that

$$f_s d A_s + f_p d A_p = f_c d b' x, \quad (1)$$

$$\begin{aligned} \sum M_z &= 0, \\ \gamma_0 M_d &= f_s d A_s \left( h - a_s - \frac{x}{2} \right) \\ &\quad + f_p d A_p \left( h - a_p - \frac{x}{2} \right), \end{aligned} \quad (2)$$

where  $\gamma_0$  is the structural importance coefficient, taking  $\gamma_0 = 1$ ;  $M_d$  is the ultimate bending moment; and  $F$  is the ultimate force.

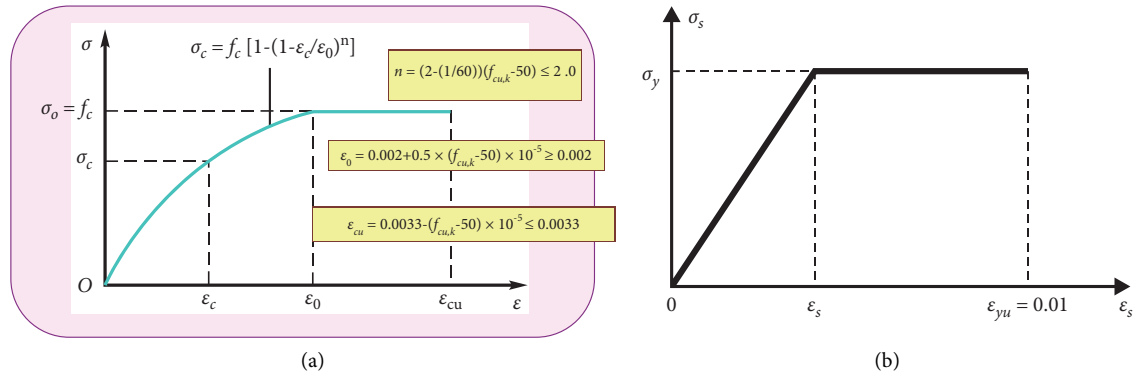


FIGURE 13: Stress-strain curve. (a) Stress-strain curve of concrete under compression. (b) Stress-strain curve of steel bar.

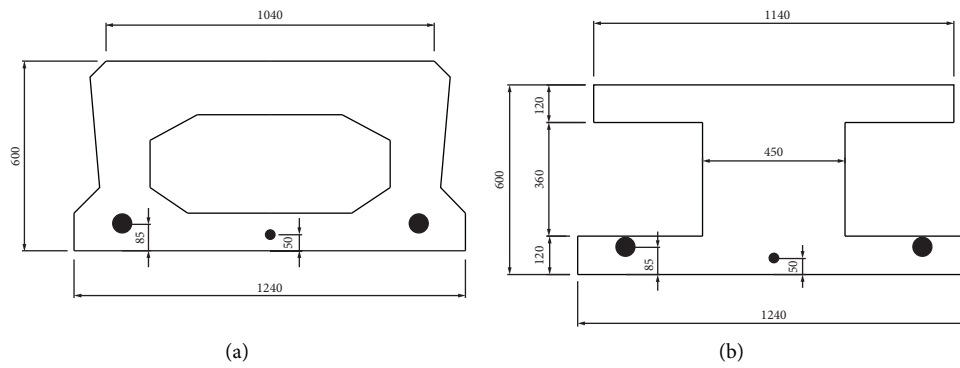


FIGURE 14: Equivalent conversion of midspan section. (a) Mid-span section of hollow slab. (b) I-section.

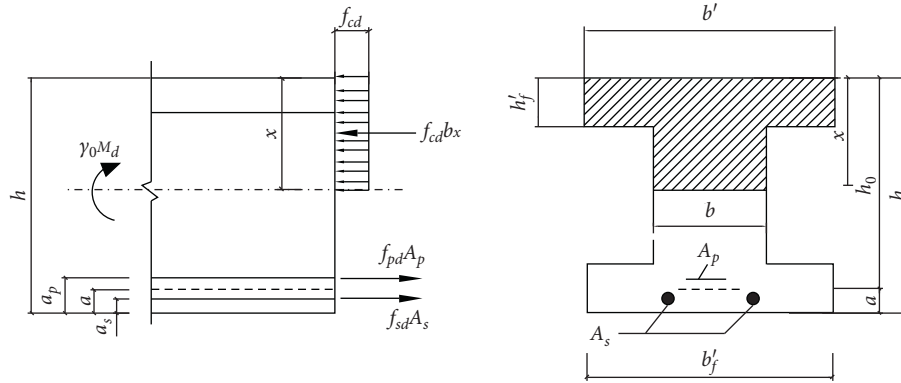


FIGURE 15: Equivalent rectangular stress figure of compression zone.

From equations (1) and (2), it follows that

$$x = \frac{f_s d A_s + f_p d A_p}{f_c d b'}$$

$$M_d = f_s d A_s (h - a_s - (x/2)) + f_p d A_p (h - a_p - (x/2)),$$

$$F = \frac{2M}{L} = 2 \frac{f_s d A_s (h - a_s - (x/2)) + f_p d A_p (h - a_p - (x/2))}{L}, \quad (3)$$

by which the bearing capacities of samples S1, S2, and S3 can be calculated. Comparisons of calculation and test results of ultimate bearing capacity are shown in Table 4:

According to Table 4, compared with Specimen S1, the ultimate bearing capacities of Specimens S2 and S3 are increased 18.5% and 33.9%, respectively, with the ultimate bearing capacity measured in the test being larger than that calculated theoretically when not considering the effect of structural reinforcement in the compression area and the tensile capacity of concrete in the tensile stress area; as a result, the theoretically calculated bearing capacity is smaller than the test result. However, the trend of theoretical calculation is consistent with the experimental results, showing that UHPC strengthening can improve the bearing capacity, bending stiffness, and deformation resistance of a prestressed concrete hollow slab, helping strengthen it. At the

TABLE 4: Comparison of calculation and test results of ultimate bearing capacity.

Specimens	Calculation results (kN)	Increase efficiency of calculation results	Test results (kN)	Increase efficiency of test results
S1	820	—	838	—
S2	972	18.5%	1,017	21.4%
S3	1,098	33.9%	1,060	26.5%

same time, the stiffness and deformation capacity of Specimens S2 and S3 are significantly improved.

4.2. *Calculation of Cracking Load.* Calculation of cracking load is based on stress distribution diagrams, as shown in Figure 16. The cracking bending moment is  $M_{cr}$ ,  $X_{cr}$  is the

height of compression zone when the crack is about to appear,  $\epsilon_{tu}$  is the ultimate tensile strain of concrete,  $E'_t$  is the tensile elastic modulus of concrete, and  $E'_t = 0.5E_c$ , where  $E_c$  is the compressive elastic modulus of concrete.

$\sum F_x = 0$ , it is obtained that

$$\sigma_s A_s + \sigma_p A_p + f_{tk} b (h - X_{cr}) + f_{tk} (b_f - b) h_f = \frac{1}{2} \sigma_c b X_{cr} + \frac{2X_{cr} - h_f}{2X_{cr}} \sigma_c h_f (b'_f - b), \quad (4)$$

after which

$$X_{cr} = \frac{2(\alpha_E A_s + \alpha_p A_p) h + (b_f - b) h_f h + b h^2 + h_f^2 b'_f - b h_f^2}{2b_f h_f + b'_f h_f + 2bh + 2(\alpha_E A_s + \alpha_p A_p) - 2bh_f - bh'_f} \quad (5)$$

$$\sum M_z = 0,$$

$$M_{cr} = \frac{X_{cr}^2}{h - X_{cr}} b f_{tk} \frac{2}{3} X_{cr} + \frac{2X_{cr} - h_f}{h - X_{cr}} h_f (b'_f - b) \frac{(h - h_f)}{2} + f_{tk} b (h - X_{cr}) \frac{(h - X_{cr})}{2} + f_{tk} (b_f - b) h_f \frac{(h - h_f)}{2} + 2\alpha_E A_s f_{tk} (h - X_{cr} - a_s) + 2\alpha_p A_p f_{tk} (h - X_{cr} - a_p), \quad (6)$$

where  $\alpha_E = (E_s/E_c)$  is the ratio of the elastic modulus of reinforcement to the elastic modulus of concrete, and  $\alpha_p = (E_p/E_c)$  is the ratio of the elastic modulus of steel strand to the elastic modulus of concrete.

The neutral axis position of Specimens S1, S2, and S3 and cracking load  $o$  can be calculated by formulas (5) and (6), as shown in Table 3:

Because the carbon fiber is only 0.167 mm, its contribution to section stiffness is not considered. At the same time, the section roof and webs are reinforced only according to the structural requirements, with this part of the steel bar's contribution to the section stiffness not considered for the converted section area and the moment of inertia. The calculation results show that the section stiffness of a UHPC-strengthened prestressed concrete hollow slab is better than that in unreinforced specimens, with cracking load being increased 58.9%.

## 5. The Finite Element Analysis

The numerical analysis was conducted using ABAQUS to better understand the flexural behaviour of hollow slab strengthened by UHPC. The numerical model was

established and validated on the basis of test results previously presented.

5.1. *The Numerical Calculation.* The C45 concrete was modeled using element C3D8R and plastic damage model. Stress-strain curve of concrete under compression is shown in Figure 13(a). The UHPC was modeled using element C3D8R. With respect to the constitutive law of UHPC, the stress-strain relationship in tension and compression had been chosen according to experiment, as shown in Table 5. There were prestressed steel strand and the steel bars using element T3D2. The carbon fiber was modeled using S4R shell element, and the tensile strength is 3500 MPa. The stress-strain relationship of the prestressed steel and the carbon fiber is shown in Figure 17, and the stress-strain curve of steel bar is shown in Figure 13(b). The finite element model of hollow slab strengthened by UHPC is shown in Figure 18. The reinforcement mesh is built into concrete using embedded commands, and the equivalent lowering temperature method was studied to simulate prestress.

For the calculation model, the slip of UHPC and C45 concrete is not considered, the constraint is binding, the displacement loading is adopted, and the calculation shows that the

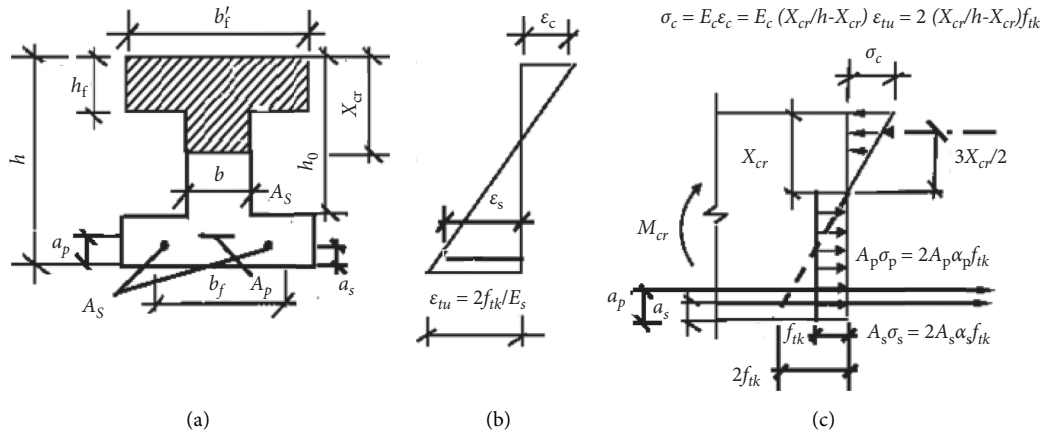


FIGURE 16: Stress distribution diagrams. (a) Section. (b) Strain distribution. (c) Stress distribution.

TABLE 5: Plastic damage parameter.

Expansion angle	Eccentricity	$f_{b0}/f_{c0}$	$K$	Stickiness parameter
30	0.1	1.16	0.667	0.0005

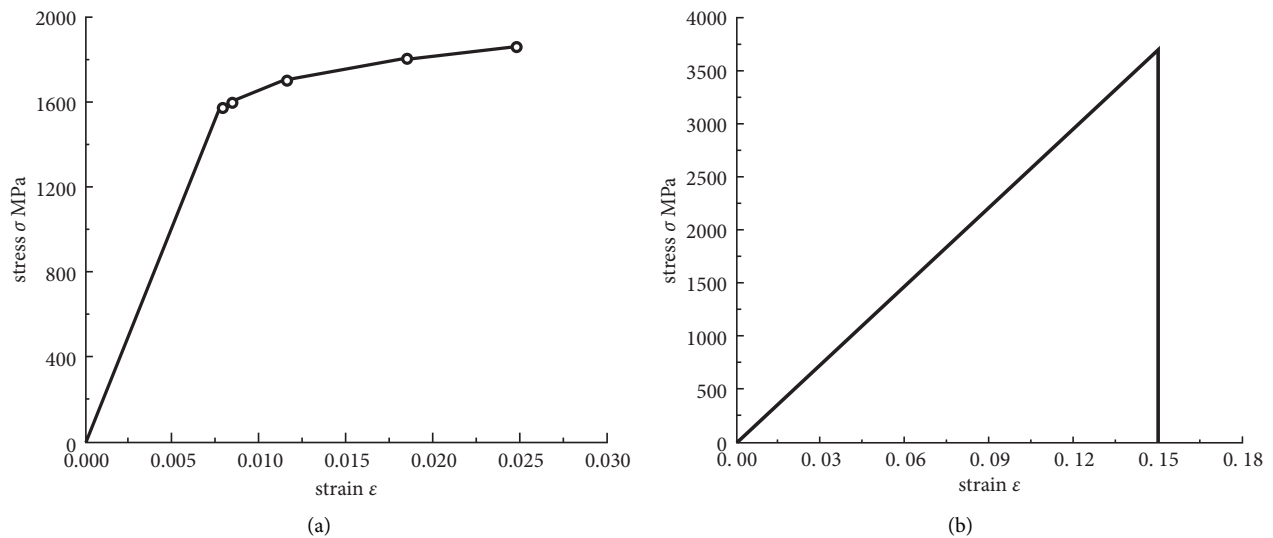


FIGURE 17: Stress-strain curve of prestressed steel strand and carbon fiber. (a) Prestressed steel strand. (b) Carbon fiber.

prestress of 1395 MPa corresponds to a temperature of  $-596^{\circ}\text{C}$ . The failure mode is shown in Figure 19. With the increase of load, the mid-span deflection gradually increases. The tensile concrete does not bear the load. Finally, the tensile reinforcement in the pure bending section of UHPC-reinforced hollow slab reaches the yield strength, the steel strand reaches the tensile strength, and the compressed concrete is crushed. The calculation model is at the ultimate flexural bearing capacity.

**5.2. Analysis of Calculation Results.** The comparison between the load-mid-span deflection results obtained from the numerical analysis and experiment test is shown in Figure 20, and the bearing capacity of hollow slab strengthened by UHPC obtained through numerical calculation, theoretical calculation, and test is shown in Table 6.

From Figure 20, it can be seen that, in the elastic stage, the numerical results are very consistent with the test results. After cracking, the specimen enters the elastic-plastic stage. There is a certain error between the numerical results and the test results, and the discreteness of concrete after cracking has a great influence. The difference between the finite element calculation results and the test results is small, and ABAQUS finite element simulation is relatively reliable.

Table 6 shows that the error between the numerical value of bearing capacity and the formula calculation value is within 3%, and the error between the numerical value of bearing capacity and the test value is within 8%, indicating that the theoretical calculation results are in good agreement with the test results. The coincidence of bearing capacity values shows that the scheme of strengthening hollow slab with shear studs connecting UHPC and

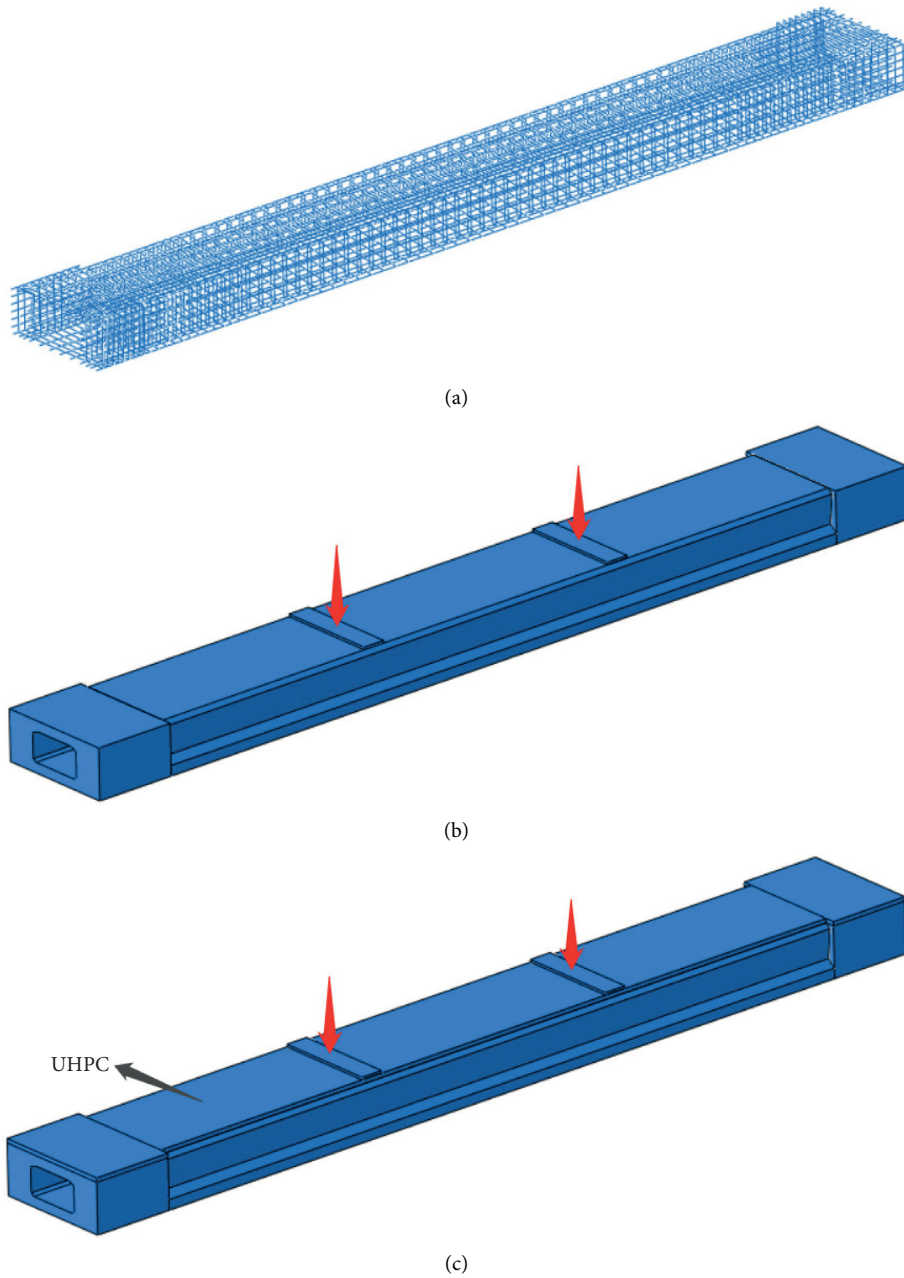


FIGURE 18: The finite element model of hollow slab strengthened by UHPC. (a) The reinforcement mesh. (b) Hollow slabs. (c) The hollow slabs strengthened by UHPC.

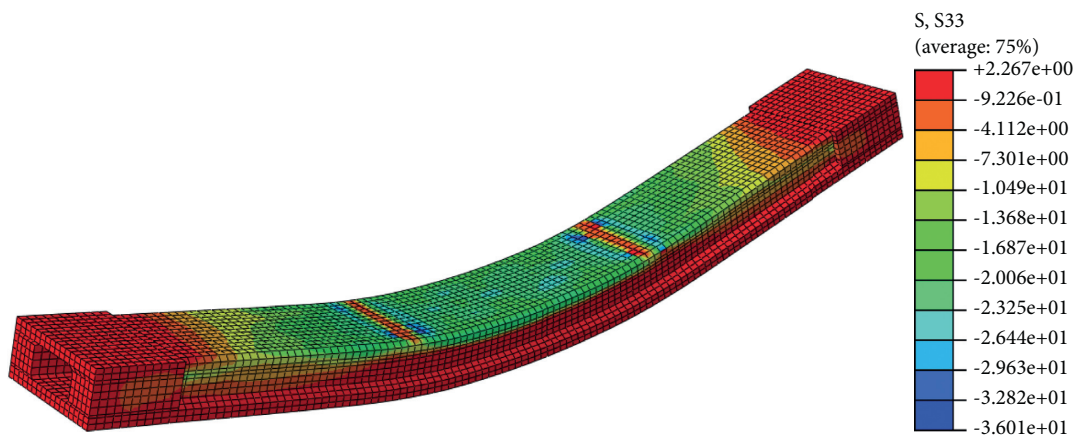


FIGURE 19: The failure mode of hollow slab strengthened by UHPC.

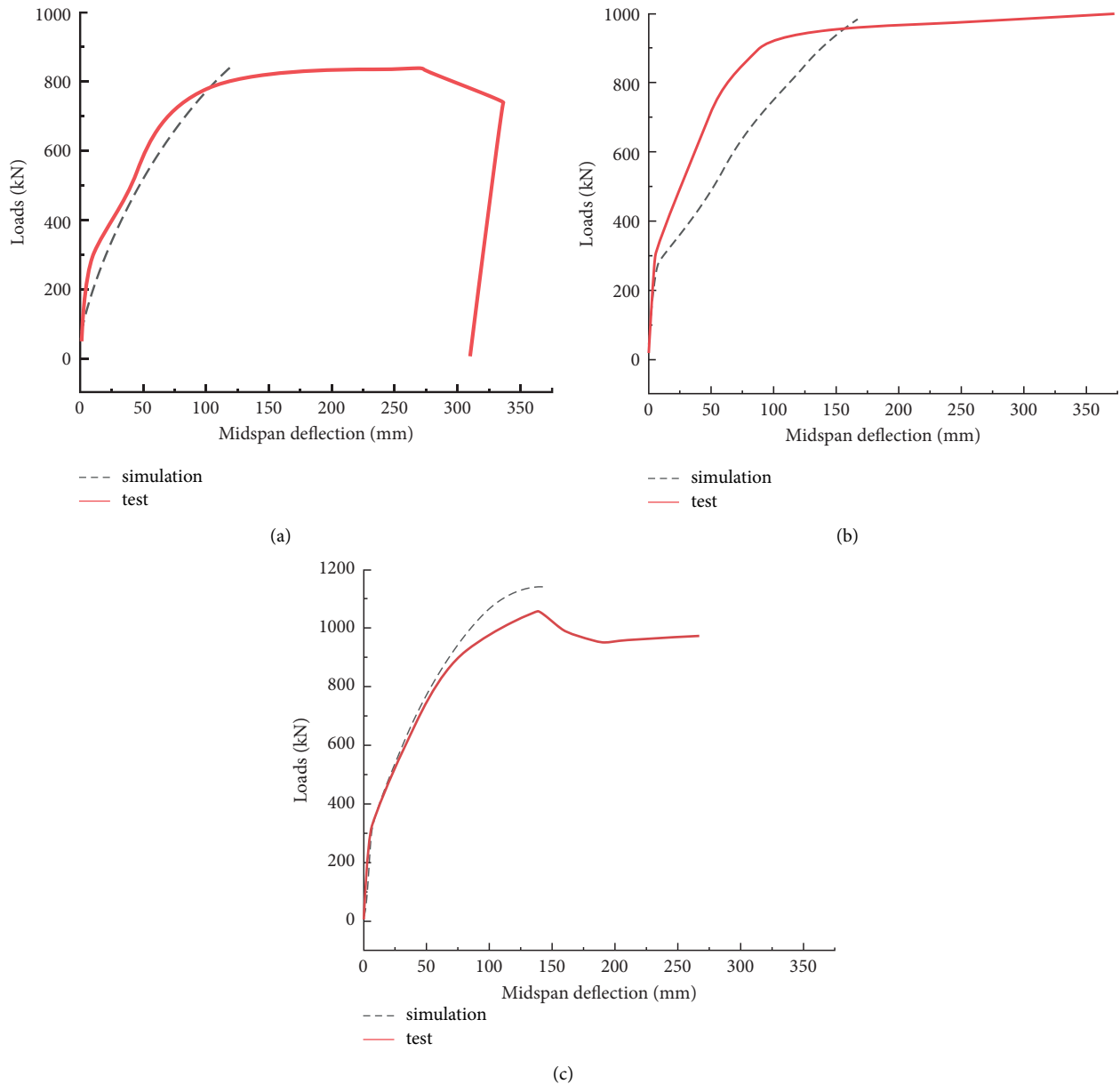


FIGURE 20: Calibration of hollow slabs analysis with test results. (a) Sample S1. (b) Sample S2. (c) Sample S3.

TABLE 6: Comparison of bearing capacity.

Specimens	Strengthened	Bending capacity (kN)				
		Numerical analysis ①	Calculation results ②	Test results ③	①/②	1/③
S1	Nonstrengthened	842	820	838	1.02	1.00
S2	UHPC	980	972	1017	1.01	0.96
S3	UHPC + CFRP	1142	1098	1060	1.04	1.08

prestressed concrete hollow slab is completely feasible. The numerical simulation are reliable and accurate.

## 6. Conclusions

This paper introduced a method of using UHPC to strengthen a prestressed concrete hollow slab. Full-scale

model load tests without strengthened prestressed concrete hollow slab, UHPC-strengthened hollow slab, and UHPC- and CFRP-strengthened hollow slab were carried out, with the following notable results:

- (1) In four-point bending full-scale model tests of Specimens S1, S2, and S3, two strengthening methods (UHPC strengthening and UHPC plus

CFRP strengthening of prestressed concrete hollow slab) significantly improved the ultimate bearing capacity of prestressed concrete hollow slabs, with the ultimate bearing capacity of the two strengthening methods increased 21.4% and 26.5%, respectively. Under 800 kN load, the midspan deflection of the UHPC-strengthened prestressed concrete hollow slab was about 45.8% lower than that of the without strengthened prestressed concrete hollow slab. The specimens all showed flexural capacity failure, indicating that UHPC strengthening is an effective method of improving the bearing capacity of prestressed concrete hollow slabs.

- (2) Prestressed concrete hollow slabs strengthened by two methods showed good composite effect in the test process, with exceptionally good integrity of the connection part.
- (3) Two strengthening methods improved crack inhibition to a certain extent, slowing crack propagation and increasing cracking load 50%. Under 800 kN load, the crack width of the prestressed concrete hollow slab strengthened by two methods decreased 56.3% and 69%, respectively. When cracks reached 0.2 mm, the load was 0.45–0.47 of the ultimate bearing capacity. CFRP has little effect on initial cracking load but can prevent crack propagation.
- (4) Calculations of ultimate bearing capacity and cracking load produce findings consistent with the test results, with UHPC strengthening significantly increasing the flexural capacity and bending stiffness of prestressed concrete hollow slabs, improving deformation resistance and crack inhibition, and effectively strengthening the tensile strength of steel bars in the tensile stress area of beams, reducing midspan deflection and steel bar strain in hollow slabs.
- (5) The numerical model satisfactorily captured both stiffness and ultimate strength of the composite beams. According to the validation presented above, it can be deduced that the results of the numerical simulation are reliable and accurate.

## Data Availability

All the data used to support the findings of this study are available from the corresponding author upon request.

## Conflicts of Interest

The authors declare that they have no conflicts of interest.

## Acknowledgments

This research was supported by the Open Projects Foundation (No. BHSKL19-04-KF) of State Key Laboratory for Health and Safety of Bridge Structures. This research was funded by the State Key Laboratory for Health and Safety of Bridge Structures (BHSKL19-04-KF). The authors would like to express their appreciation for this financial assistance.

## References

- [1] B. Khaleghi, E. Schultz, S. Seguirant et al., “Accelerated bridge construction in Washington State: from research to practice,” *PCI Journal*, vol. 57, no. 4, pp. 34–49, 2012.
- [2] S. S. Badie, M. R. Kamel, and M. K. Tadros, “Precast pre-tensioned trapezoidal box beam for short span bridges,” *PCI Journal*, vol. 44, no. 1, pp. 48–59, 1999.
- [3] U. Attanayake, O. Abudayyeh, J. Cooper, A. W. Mohammed, and H. Aktan, “First full-depth deck-panel accelerated bridge construction project in Michigan: constructability challenges and lessons learned,” *Journal of Performance of Constructed Facilities*, vol. 28, no. 1, pp. 128–135, 2014.
- [4] O. Abudayyeh, H. Cai, B. Mellema, and S. Yehia, “Quantifying time and user cost savings for rapid bridge construction technique,” *Transportation Research Record: Journal of the Transportation Research Board*, vol. 2151, no. 1, pp. 11–20, 2010.
- [5] M. Tazarv, L. Bohn, and N. Wehbe, “Rehabilitation of longitudinal joints in double-tee girder bridges,” *Journal of Bridge Engineering*, vol. 24, p. 6, Article ID 04019044, 2019.
- [6] Q. T. Su, G. T. Yang, and M. A. Bradford, “Behavior of a continuous composite box girder with a prefabricated prestressed-concrete slab in its hogging-moment region,” *Journal of Bridge Engineering*, vol. 20, no. 8, 13 pages, 2015.
- [7] I. De la Varga, R. P. Spragg, J. F. Munoz, M. A. Helsen, and B. A. Graybeal, “Cracking, bond, and durability performance of internally cured cementitious grouts for prefabricated bridge element connections,” *Sustainability*, vol. 10, no. 11, p. 21, 2018.
- [8] L. Macorini, M. Fragiacomio, C. Amadio, and B. A. Izzuddin, “Long-term analysis of steel-concrete composite beams: FE modelling for effective width evaluation,” *Engineering Structures*, vol. 28, no. 8, pp. 1110–1121, 2006.
- [9] F. Ceroni, “Experimental performances of RC beams strengthened with FRP materials,” *Construction and Building Materials*, vol. 24, no. 9, pp. 1547–1559, 2010.
- [10] B. Zhu, Z. Lu, and H. Wu, *Damage Detection and Strengthening for Building Structures*, Tongji University Press, Shanghai, China, (in Chinese), 1995.
- [11] B. J. Bett, R. E. Klingner, and O. J. James, “Lateral load response of strengthened and repaired reinforced concrete columns,” *ACI Structural Journal*, vol. 85, no. 5, pp. 499–508, 1988.
- [12] E. Brühwiler, “Swiss standard SIA-2052. UHPFRC: materials, design and application,” in *Proceedings of the 4th International Symposium on Ultra-High Performance Concrete and High Performance Materials*, Kassel, Germany, March 2016.
- [13] E. Brühwiler, “UHPFRC technology to enhance the performance of existing concrete bridges,” *Structure and Infrastructure Engineering*, vol. 16, no. 1, pp. 94–105, 2020.
- [14] H. Martín-Sanz, K. Tatsis, D. Damjanovic et al., “Getting more out of existing structures: steel bridge strengthening via UHPFRC,” *Frontiers in Built Environment*, vol. 5, no. 26, pp. 1–20, 2019.
- [15] E. Brühwiler, ““Structural UHPFRC”: welcome to the post-concrete era !” in *Proceedings of the First International Interactive Symposium on UHPC*, Des Moines, IA, July 2016.
- [16] E. Brühwiler and E. Denarié, “Rehabilitation and strengthening of concrete structures using ultra-high performance fibre reinforced concrete,” *Structural Engineering International*, vol. 23, no. 4, pp. 450–457, 2013.
- [17] E. Denarié and E. Brühwiler, “Structural rehabilitations with ultra-high performance fiber reinforced concretes

- (UHPC),” *Restoration of Buildings and Monuments*, vol. 12, no. 5/6, pp. 453–468, 2006.
- [18] M. A. Al-Osta, M. N. Isa, M. H. Baluch, and M. K. Rahman, “Flexural behavior of reinforced concrete beams strengthened with ultra-high performance fiber reinforced concrete,” *Construction and Building Materials*, vol. 134, pp. 279–296, 2017.
- [19] K. M. Zmetra, K. F. McMullen, A. E. Zaghi, and W. Kay, “Experimental study of UHPC repair for corrosion-damaged steel girder ends,” *Journal of Bridge Engineering*, vol. 22, no. 8, Article ID 04017037, 2017.
- [20] Z. B. Haber, J. F. Munoz, and B. A. Graybeal, *Field Testing of an Ultra-high Performance Concrete Overlay*. FHWA-HRT-17-096, United States Department of Transportation, Federal Highway Administration, Washington, D.C., U.S, 2017.
- [21] G. Doiron, “Pier repair/retrofit using UHPC-examples of completed projects in North America,” in *Proceedings of the First International Interactive Symposium on UHPC*, Des Moines, Iowa, July 2016.
- [22] X. Wu and Y. Lin, “Flexural behavior of UHPC-RC composite beam,” *Steel and Composite Structures*, vol. 22, no. 2, pp. 387–398, 2016.
- [23] D. Qi, *Research on Flexural Behavior of UHPC Strengthened Damaged Plates*, Hunan University, Changsha, China, 2016.
- [24] C. Liu, Y. Zou, and Z. Zhao, “Comparison and selection of reinforcement schemes for hollow slab girder bridge of Tongji Road overpass,” *Bridge Construction*, vol. 48, no. 4, pp. 118–123, 2018.
- [25] Z. Deng and W. Zhang, “Flexural behavior of concrete beams strengthened with hybrid fiber reinforced RPC,” *Journal of Harbin Engineering University*, vol. 9, no. 36, pp. 1199–1205, 2015.
- [26] J. Yang and F. Zhi, “Study on flexural behavior of prestressed ultra high performance concrete beams,” *Chinese Journal of highway*, vol. 22, no. 1, pp. 39–46, 2009.
- [27] D. Zhang, Z. Zhi, Z. Lu et al., “Experimental study on flexural capacity of cast-in-place RC beams with prefabricated core,” *Engineering Mechanics*, vol. 26, no. 5, pp. 164–170, 2009.
- [28] Y. P. Zhu, Y. Zhang, H. H. Hussein, and G. D. Chen, “Flexural strengthening of reinforced concrete beams or slabs using ultra-high performance concrete (UHPC),” *A state of the art review. Eng. Struct.*, vol. 205, Article ID 110035, 19 pages, 2020.